OXFORD

Psychoradiology, 1(2), 2021, 73–87

https://doi.org/10.1093/psyrad/kkab007
Research article

RESEARCH ARTICLE

Motor adaptation and internal model formation in a robot-mediated forcefield

Myriam Taga [1,*], Annacarmen Curci[1], Sara Pizzamigglio[2], Irene Lacal[2], Duncan L. Turner[1] and Cynthia H.Y. Fu[3,4]

[1]School of Health, Sports and Bioscience, University of East London, London, UK
[2]Department of Computer Science, School of Architecture, Computing and Engineering, University of East London, London, UK
[3]Department of Physiology and Pharmacology, Sapienza University, Rome, Italy
[4]School of Psychology, University of East London, London, UK
[5]Centre for Affective Disorders, Institute of Psychiatry, Psychology and Neuroscience, King's College London, London, UK

*Correspondence: Myriam Taga, myriam.taga@nyulangone.org

Abstract

Background: Motor adaptation relies on error-based learning for accurate movements in changing environments. However, the neurophysiological mechanisms driving individual differences in performance are unclear. Transcranial magnetic stimulation (TMS)-evoked potential can provide a direct measure of cortical excitability.
Objective: To investigate cortical excitability as a predictor of motor learning and motor adaptation in a robot-mediated forcefield.
Methods: A group of 15 right-handed healthy participants (mean age 23 years) performed a robot-mediated forcefield perturbation task. There were two conditions: unperturbed non-adaptation and perturbed adaptation. TMS was applied in the resting state at baseline and following motor adaptation over the contralateral primary motor cortex (left M1). Electroencephalographic (EEG) activity was continuously recorded, and cortical excitability was measured by TMS-evoked potential (TEP). Motor learning was quantified by the motor learning index.
Results: Larger error-related negativity (ERN) in fronto-central regions was associated with improved motor performance as measured by a reduction in trajectory errors. Baseline TEP N100 peak amplitude predicted motor learning ($P = 0.005$), which was significantly attenuated relative to baseline ($P = 0.0018$) following motor adaptation.
Conclusions: ERN reflected the formation of a predictive internal model adapted to the forcefield perturbation. Attenuation in TEP N100 amplitude reflected an increase in cortical excitability with motor adaptation reflecting

Received: 13 January 2021; **Revised:** 28 April 2021; **Accepted:** 15 May 2021

neuroplastic changes in the sensorimotor cortex. TEP N100 is a potential biomarker for predicting the outcome in robot-mediated therapy and a mechanism to investigate psychomotor abnormalities in depression.

Key words: EEG; TMS; motor adaptation; robot-mediated forcefield; N100; ERN

Introduction

Goal-directed reaching relies on complex neural motor commands to achieve the desired goal and trajectory. The mechanism relies on inverse models making transformations from the desired movement trajectory in the visual space to motor commands in the motor space (Wolpert *et al.*, 1998), and by integrating motor commands with sensory feedback mechanisms (Shadmehr *et al.*, 2010; Scott *et al.*, 2015). This adaptive internal model of the body and world enables flexible and accurate movements.

Motor adaptation refers to the learning of a previously known motor skill in the presence of an additional perturbation. Error signals play a key role in aiding the motor system to make smooth movement corrections (Desmurget and Grafton 2000; Diedrichsen *et al.*, 2005), and motor adaptation is a form of motor learning during which sensory prediction errors are used to recalibrate internal models. Mismatches between predictions and actual sensory outcomes are used as feedback error signals to update subsequent motor commands (Scott *et al.*, 2015). The generated corrective responses that are adapted to the new environment then update the internal models to predict the sensory consequences of the motor behaviour (Haith and Krakauer 2013). Typical experimental paradigms include serial response tasks, visuomotor rotation, and forcefield learning tasks (Krakauer and Mazzoni 2011).

Spatiotemporal neural dynamics of error processing have been investigated through the recording of event-related potentials (ERPs) using electroencephalographic (EEG) activity (Falkenstein *et al.*, 1995). The negative ERP component that peaks around the timing of an error commission has been termed error-related negativity (ERN) and is believed to originate in the anterior cingulate cortex (ACC) (Gehring *et al.*, 2018). ERN is proposed to be involved in the modification of internal models in motor adaptation (Contreras-Vidal and Kerick 2004; Torrecillos *et al.*, 2014). In a serial reaction time task, Beaulieu *et al.* (2014) found that the change in ERN amplitude over the course of the task correlated with motor sequence learning. ERN could be an electrophysiological marker for the development of cognitive control efficiency in motor sequence learning; however, it has not been examined during motor adaptation in a forcefield learning paradigm.

Cortical plasticity is a crucial mechanism for continuously adapting movements to a changing environment and is involved in error-based learning (Ostry and Gribble 2016). Modulations in cortical excitability reflect short-term functional neuroplasticity change, which might underlie motor adaptation. The interaction with novel forcefields during a robot-mediated task is proposed to lead to the formation of an internal model that can be generalized to unconstrained movement (Patton and Mussa-Ivaldi, 2004; , Patton et al., 2006).

Baseline beta power and resting state connectivity have been associated with subsequent motor adaptation performance. Higher rates of adaptation were predicted by lower baseline beta oscillatory power (Ozdenizci *et al.*, 2017) as well as resting state functional connectivity between the contralateral M1 and anterior prefrontal cortex (Faiman *et al.*, 2018).

Transcranial magnetic stimulation (TMS) can trigger and modulate neural activity through an electric current that has been induced by an external time-varying magnetic field (Ridding and Rothwell 2007). To study corticospinal pathways, TMS is applied to the motor cortex (M1) and motor evoked potentials (MEP) in the targeted muscle have been recorded with electromyography (EMG) (Ziemann 2017). However, MEPs reflect both the state of neurons in M1 as well as in the spinal cord and muscle properties; thus, the term corticospinal activity is commonly used to highlight the indiscriminability of MEPs between cortical and spinal influences.

Cortical evoked potentials measured with EEG quantify not only corticospinal but also direct cortical excitability. Combining TMS with EEG allows the identification of cortical biomarkers of movement control, which can be measured independently from the integrity of the corticospinal tract. Single-pulse TMS applied over M1 produces a well-characterized negative deflection, called TEP N100, which has been established as a biomarker of inhibitory processes, reflecting the activity of $GABA_B$ receptors whereby a larger N100 amplitude reflects increased inhibition and a small amplitude reflects decreased inhibition (Bonnard *et al.*, 2009; Premoli *et al.*, 2014; Spieser *et al.*, 2010). TEP N100 amplitude measures cortical excitability and provides an indirect measure of plasticity by quantifying changes in TEP amplitudes (Farzan *et al.*, 2016).

This present study applied a robot-mediated upper limb reaching task in an unperturbed (non-adapting condition) and in a forcefield perturbed (adapting condition) environment with simultaneous EEG recording to identify the neural correlates and biomarkers of error-based learning. TMS was applied to the contralateral (left) M1 cortex immediately before and after the motor adaptation condition, and EEG was acquired to measure cortical excitability linked to motor performance. Applying a highly standardized robot-mediated reaching task provides high measurement reliability and controllability in upper limb reaching tasks representing a highly standardized assessment of the motor system (Pizzamiglio *et al.*, 2017).

Adaptation to the applied forcefield was expected, which would be evident in temporary after effects following removal of the forcefield with an eventual return to a baseline performance. We expected that ERN during motor adaptation would correlate with motor learning, and cortical excitability would be modulated, reflecting neuroplastic changes that would be evident in decreases in TEP N100 amplitudes following motor adaptation. If cortical excitability at rest, before motor adaptation, is linked to individual variability in motor learning capacity, then we expected that the TEP N100 amplitude as an inhibitory biomarker would be predictive of subsequent motor learning.

Materials and Methods

Participants

Participants were 15 healthy adults [mean age ± standard deviation (SD) = 23 ± 4 years, age range: 19–32 years; 8 female]. All participants provided written informed consent. The study was approved by the University of East London Ethics Committee (UREC 1718/03) and was conducted according to the Declaration of Helsinki. Participants were assessed for any contraindications to TMS (Rossi *et al.*, 2009). All participants were right-handed as assessed by Edinburgh Handedness Inventory (Oldfield, 1971) and had normal or corrected to normal vision. Participants did not have any history of neurological or psychiatric disorders, physical disability, or substance use.

Experimental task and design

Participants performed visually triggered reaching movements with their dominant (right) arm rested in a robotic manipulandum (IMT2, Interactive Motion Technologies, Cambridge, MA, USA). In each trial, participants performed a voluntary movement with the right arm to a north-west oriented target on presentation of the visual cue from a central position followed by a passive robot-assisted return to the starting position. Before each trial, participants held the joystick within the starting central circle and waited for a visual cue. Movement initiation was then indicated by the peripheral target turning from red to yellow. The intertrial interval was 6 s.

There were three experimental conditions: (i) familiarization (FAM), (ii) motor adaptation, and (iii) wash out. There were 288 trials in total, and each condition was composed of four blocks of 24 trials. During the familiarization and wash-out conditions, the reaching movement was performed under a null field. In the motor-adaptation condition, the robot applied a velocity-dependent forcefield in the clockwise direction of +25 Newton seconds per metre (Ns/m) absolute intensity, perpendicular to the trajectory of the joystick. After each block of 24 trials, a break of 1 minute was given. EEG was continuously recorded during each condition (Faiman *et al.*, 2018) (Fig. 1).

Following the familiarization condition, 50 single-pulse TMS were administered to the left M1 targeting the right (task arm) at rest premotor adaptation (Supplementary Methods, TMS Targeting). Following motor adaptation, the same TMS protocol was repeated post and followed by the wash-out condition.

Data acquisition

Kinematic measures

Kinematic measures and neural activity were recorded simultaneously. Kinematic measures were obtained from recordings of the angular position of the two robotic joints extracted to determine the position (m) and velocity (m/s) of the end effector in the horizontal plane (along the *x* and *y* axes) and forces exerted (along the *x*, *y*, and *z* axes) with a sampling rate of 200 Hz.

EEG measure of neural activity

EEG activity was recorded using a high density 64-channel Waveguard cap (ANT Neuro, Entschede, Netherlands), including one ground electrode (AFz) and one reference electrode (CPz). EEG electrodes were arranged on the cap using the 10–10 system. The positioning of the electrodes was according to the international 10–20 system (Jasper, 1958) extended to 64 electrodes. The signal was amplified using a TMS-compatible DC amplifier, the eego^{TM} sports system (ANT Neuro, Enschede, Netherlands) with a sampling frequency of 1024 Hz.

TMS-EEG measure of neural activity

To assess cortical excitability pre- and post-motor adaptation, 50 single-pulse TMS were applied pre-and post-motor adaptation to the left M1 at 100% resting motor threshold (RMT) at rest. The interstimulus interval between TMS pulses was on average 5 s with a random intertrial interval variation of 20% to reduce anticipation of the next trial. To minimize the auditory evoked potentials resulting from the TMS discharge, participants listened to white noise played through ear plugs, at less than <70 dB in each ear, for the duration of the TMS session.

During SP TMS stimulation, EEG data were continuously recorded at a sampling frequency rate of 2048 Hz, amplified by an EEG GoPro amplifier (ANT Neuro, Entschede, Netherlands). Raw EMG signals were sampled at 5 kHz with a Micro CED 1401 analogue-to-digital laboratory interface (Cambridge Electronics Design, UK), amplified, and filtered (bandpass filter 45 Hz high pass, 1 kHz low pass) with a CED 1902 amplifier (Cambridge Electronics Design, UK).

Data analysis

EEG measures of neural activity

EEG data preprocessing: EEG data from each condition were merged into one file and preprocessed together. EEG data were down sampled from 2048 to 1000 Hz. A band pass filter (1–80 Hz, zero-phase Butterworth filter, order = 4) and band stop filter (48–52 Hz, zero-phase Butterworth filter, order = 4) were applied to remove line

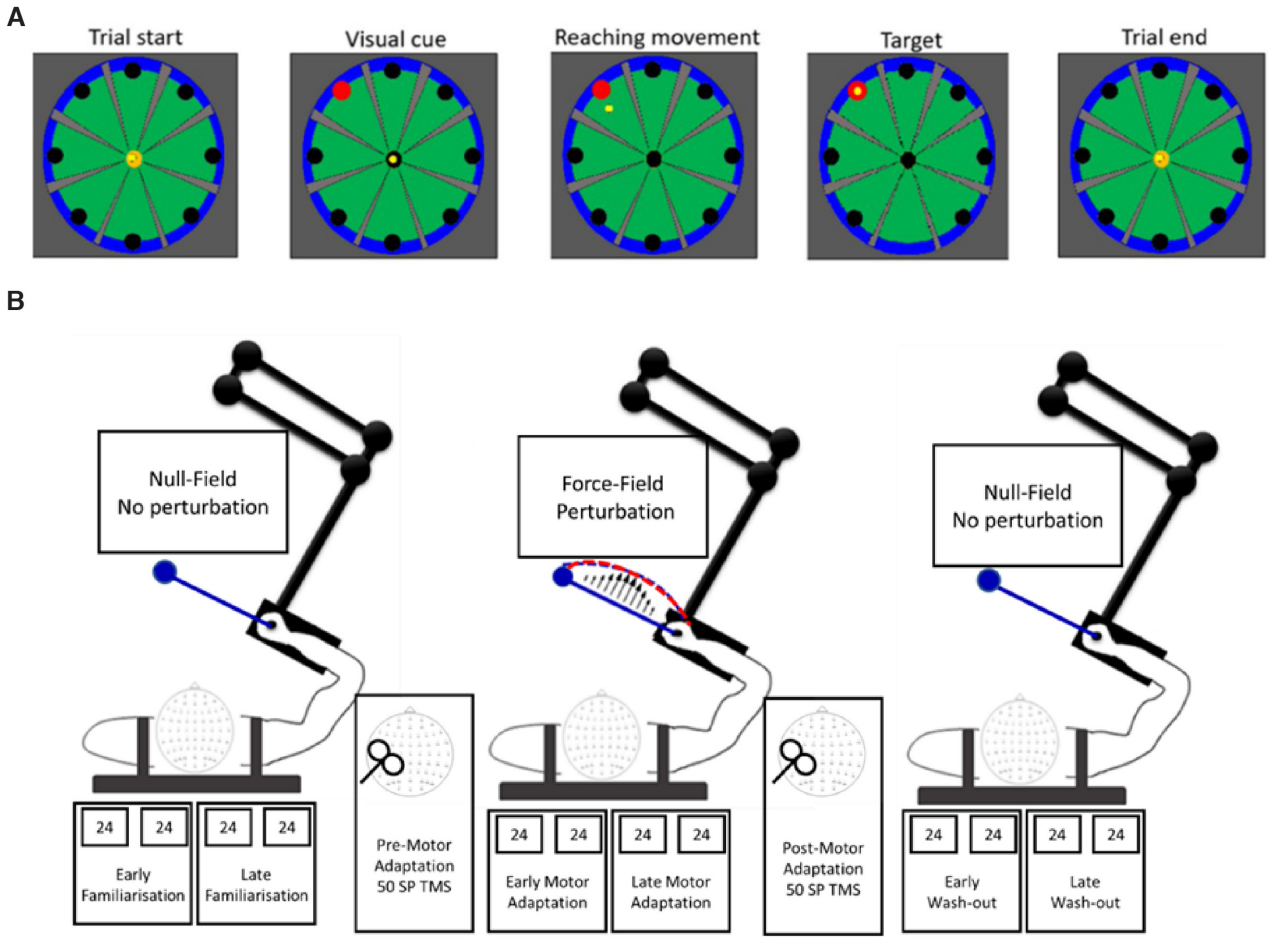

Figure 1: Experimental task and design. **(A)** The screen displays a dartboard in which a cursor (yellow dot) tracks the real-time hand position of participants and is projected on the screen. Each trial starts with the yellow cursor at the central position (orange dot). Following the appearance of the visual cue at the target circle (north-west direction), indicated by the target turning red, the participant is required to move the yellow cursor towards the target circle and hold this position until the cursor (i.e. the hand) is passively returned by the robot to the central start position. **(B)** There were three experimental conditions: familiarization, motor adaptation, and wash out. During familiarization and wash out, the robot-mediated reaching was performed in an unperturbed environment (null-field). During motor adaptation, a velocity-dependent forcefield in the clockwise direction was applied by the robot during reaching movements. Pre- and post-motor adaptation, single-pulse TMS was applied to the left M1 at rest. EEG was continuously recorded throughout the experimental task and during TMS stimulation.

noise (50 Hz). Data were epoched from −1 to 2 s around the visual cue. Electrodes and trials with mechanical artefacts were identified by means of visual inspection and rejected. On average, across participants and conditions, at least 44 artefact-free trials remained (early familiarization 46 ± 2, late familiarization 44 ± 2, early motor adaptation 44 ± 3, late motor adaptation 46 ± 2, early WO 45 ± 2, and late WO 45 ± 3) and 5 ± 2 electrodes (i.e. 8 ± 3% of total electrodes) were deleted. To remove artefacts such as eye-blinks, lateral eye movements, and electrode movements, an ICA decomposition was performed using the FASTICA algorithm (Korhonen *et al.*, 2011). Deleted electrodes were then interpolated using spherical interpolation and the data were re-referenced to common average. To examine evoked responses in the time domain, all clean trials were baseline corrected (−800 to 0 ms pre-visual cue) and then averaged for each electrode.

Event-related potentials: ERPs were calculated for late familiarization, early motor adaptation, late motor adaptation, and late wash out for each participant at each electrode. Visual inspection (Signal; Cambridge Electronics Design, UK) revealed that the fronto-central electrode site FCz showed the largest negative deflection (N300, i.e. ERN), consistent with previous findings (Gehring *et al.*, 2018; Krigolson *et al.*, 2015; MacLean *et al.*, 2015). The mean amplitude of the N300 was calculated as an average between 280 and 360 ms post visual cue.

TMS-EEG evoked responses

EEG data from both TMS conditions (pre- and post-motor adaptation) were merged into one file and preprocessed together. We used a semi-automated TMS-EEG preprocessing pipeline (i.e. TMS–EEG signal analyser (TESA), an open-source extension for EEGLAB using specific functions created for concurrent TMS–EEG analysis that minimizes artefacts while maintaining the integrity of the neural system (Mutanen *et al.*, 2020; Rogasch et al., 2014; Rogasch *et al.*, 2017). Data were epoched (−1 to +2 s)

around the TMS pulse. Epochs were demeaned by subtracting the average between −1 and +2 s from each epoch to remove the DC offset. The TMS pulse artefact was removed from −2 to +10 ms around the TMS pulse and removed data were replaced with artefact-free data using data from −7 to −2 and +10 to +15 ms using cubic interpolation. EEG data were then down sampled from 2048 to 1000 Hz. Electrodes and epochs with mechanical artefacts were identified by means of visual inspection and rejected. After this step, each condition contained at least 45 artefact-free trials. The premotor adaptation condition contained 45 ± 6 and the post-motor adaptation condition contained 46 ± 2 on average across participants. On average, across participants, 4 ± 2 electrodes (i.e. 6 ± 3% of total electrodes) were deleted.

Data were then submitted to ICA decomposition using the FASTICA algorithm (Korhonen *et al.*, 2011) and components representing the decay artefact caused by the TMS evoked muscle activity from the stimulation of scalp muscles were identified and rejected (Supplementary Fig. 1). On average, across participants, 4 ± 2 components (i.e. 7 ± 3% of total ICA components) were rejected. Data between −2 and +15 ms around the TMS pulse were removed and replaced with artefact-free data using data from −7 to −2 and +15 to +20 ms that used cubic interpolation. A bandpass filter (1–80 Hz, zero-phase Butterworth filter, order = 4) and band stop filter (48–52 Hz, zero-phase Butterworth filter, order = 4) to remove line noise (50 Hz) were applied. A second round of ICA decomposition was performed, and remaining artefacts (eyeblinks, lateral eye movements, electrode movement, and electrical artefacts) were identified and removed (Supplementary Fig. 1). On average, across participants, 30 ± 5 components (i.e. 51 ± 9% of total ICA components) were rejected. Deleted electrodes were interpolated using a spherical interpolation and the data were re-referenced to the common average (Supplementary Fig. 1).

To examine TMS-evoked responses in the time domain, all clean trials were baseline corrected (−800 to −100 ms pre-TMS). TEPs were then calculated for each participant, condition (pre- and post-motor adaptation), and electrode as simple mathematical averages across trials.

To investigate how motor adaptation modulated cortical excitability (pre- versus post-motor adaptation) and to investigate whether premotor adaptation cortical excitability predicted motor learning, peak amplitude of the N100 TEP component was extracted in the time window of 75–150 ms based on the TEP butterfly plot and in line with previous TMS-EEG literature (Farzan *et al.*, 2013; Komssi *et al.*, 2004; Paus *et al.*, 2001). TEP peak analysis was performed in every electrode using the tep_extract function of the TESA toolbox (Rogasch *et al.*, 2017). Peaks were defined as a data point that is greater than (positive) or less than (negative) five data points on either side of the peak. If multiple peaks were detected within a time window, the largest peak was used. More information is available in Supplementary Methods (Data analysis, Kinematic measure of performance, and EEG measures).

Statistical analysis

ERP and kinematic trials were averaged for late familiarization, early motor adaptation, late motor adaptation, early wash out, and late wash out. Late familiarization, rather than early familiarization, was considered to be the baseline to prevent the inclusion of potential task novelty effects. Early motor adaptation was considered to reflect the early stage adaptation as these blocks encompassed the initial exposure to the forcefield and late motor adaptation to more adapted stages. Late wash out was included in the analysis to examine whether de-adaptation to the removed forcefield occurred and activity returned to baseline (Pizzamiglio *et al.*, 2017). To obtain sufficient trial counts for the ERP measures, the trials of each condition were pooled together and averaged in the following conditions, late familiarization, early and late motor adaptation, and late wash out, similar to the literature (Anguera *et al.*, 2009; Frank *et al.*, 2005; Pizzamiglio *et al.*, 2017).

Unless stated otherwise, all data were assessed using parametric statistical tests following confirmation of normal distribution of data using the Shapiro–Wilk test. All statistical procedures were performed using SPSS (IBM SPSS, v.24.0). For all statistical analyses, the level of significance was a priori set to $\alpha = 0.05$. All kinematic measures were calculated trial-by-trial for each participant.

Kinematic data analysis

From the kinematic measures, we quantified errors as the sum of the perpendicular distance (path offset) between the actual and the ideal trajectory (i.e. straight line) at each time point from movement onset to offset. To determine the degree of forcefield learning the motor learning index (MLI) (Faiman *et al.*, 2018; Ozdenizi *et al.*, 2017) was calculated for each participant. To this end, average summed errors were computed for the first five trials (T1) and for the last five trials (T2) during the motor adaptation condition and the MLI calculated as the percentage change from T1 with the following equation: $\text{MLI} = [(\text{T1} - \text{T2})/\text{T1}] \times 100$. The percentage change was chosen rather than using the difference between T1 and T2, to facilitate the comparability between this study and previous studies using the same measure to identify neural correlates of motor performance improvements (Faiman *et al.*, 2018, Ozdenizci *et al.*, 2017).

All data were assessed for normality using the Shapiro–Wilk test and sphericity using the Mauchly test. All data met the assumption for normality, however, since kinematic data violated the assumption of sphericity, a Greenhouse Geisser correction was applied for analyses of variance (ANOVAs). Multivariant ANOVA was performed with a within-participant factor of condition (late familiarization, early motor adaptation, late motor adaptation, and late wash out) with the following dependent variables: movement onset, offset, time, maximum

velocity, maximum force, and summed errors. If a significant effect was detected, ANOVAs were performed on each of the dependent variables separately. Post hoc Bonferroni-adjusted paired *t*-tests were performed for significant main effect of condition.

ERP N300 (i.e. ERN) neural activity analysis

Across conditions in the N300 amplitude were assessed using a one-way repeated-measure ANOVA with condition (late familiarization, early motor adaptation, late motor adaptation, and late wash out) as a within-participant factor.

Since the ERP statistical analysis was performed on a whole scalp (63 electrodes) level, non-parametric permutation-based repeated-measure ANOVAs (2000 permutations) were used to assess differences across conditions in each electrode for each ERP component separately. If a significant main effect of condition was found, non-parametric permutation-based paired *t*-tests, which minimize the number of false-discoveries (Fields and Kuperberg, 2018), were used to compare each condition with the late familiarization condition, as well as between early and late motor adaptation. The function statcond as implemented in EEGLAB (Delorme and Makeig, 2004) (statcond.m, 2000 permutations, $P < 0.05$ (or 0.0125 for the post hoc paired *t*-tests) (false discovery rate (FDR); Benjamini and Yekutieli, 2001), was used to determine the electrodes in which EEG outcome measures were statistically different. Specifically, each EEG outcome measure from each electrode from each participant is permuted (2000 permutations) across conditions. In this way, ANOVA or *t*-tests was performed with surrogate data (i.e. shuffle participants across conditions, which represents the null hypothesis that the conditions come from the same distribution, hence no mean difference) 2000 times. These 2000 *F* statistics form the null distribution and any electrode with a *t* or *F* value in the unpermuted data that was >95% (i.e. $P < 0.05$) of values in this null distribution was considered significant. All *P* values were FDR adjusted to control for multiple comparisons (i.e. 63 electrodes).

As the N300 component has been linked to error processing and motor learning (Anguera *et al.*, 2009; Torrecillos *et al.*, 2014) as well as to performance improvements (Beaulieu *et al.*, 2014), the correlation between the N300 amplitude in the averaged electrodes and modulation during early and late motor adaptation from late familiarization was examined in a correlation analysis between N300 amplitude and summed errors during early and late motor adaptation, as well as between the averaged N300 amplitude of early and late motor adaptation.

TMS-EEG analysis: TEP N100

The TEP N100 peak analysis was first performed on a whole scalp level and then activity of significant electrodes was averaged and used for further analysis to determine the global effect of motor adaptation. The N100 amplitude at each electrode between pre- and post-motor adaptation using permutation-based *t*-tests (2000 permutations) were compared. TEPs from significant electrodes were then averaged and the N100 amplitude was extracted pre-and post-motor adaptation.

As part of the resting-state prediction, MLI was predicted with a linear regression model with each participant's TEP N100 amplitude premotor adaptation as the independent variable.

Results

Kinematics

Changes in movement execution were observed as participants adapted to the velocity-dependent forcefield. In late familiarization trials, participants performed straight north-west movements to the target. However, as expected, at the beginning of motor adaptation, the sudden introduction of the clockwise velocity-dependent forcefield perturbation resulted in movement trajectories that considerably deviated from the ideal trajectory, resulting in curved trajectories. With repetitive exposure to the forcefield, participants were able to counteract the forces resulting in straight-lined trajectories and velocity profiles similar to those profiles during late familiarization. After the removal of the forcefield during the wash-out condition, movement trajectories showed deviations from the ideal straight line in the opposite direction as during exposure to the forcefield (after effects). Nevertheless, the movement trajectories quickly returned to pre-forcefield exposure trials with very small deviations from the straight line (Fig. 2, Supplementary Fig. 4).

There was a significant main effect on kinematic measures of condition [Pillai's trace = 1.27, $F_{(15, 120)} = 5.90$, $P < 0.0001$, $\eta^2 = 0.42$] (Supplementary Fig. 5). Repeated-measure ANOVA between conditions (late familiarization, early motor adaptation, late motor adaptation, and late wash out) showed that movement onset [$F_{(2.33, 32.55)} = 0.35$, $P = 0.74$, $\eta^2 = 0.024$], movement offset [$F_{(1.99, 27.99)} = 4.18$, $P = 0.06$, $\eta^2 = 0.23$], and movement time [$F_{(1.89, 26.47)} = 3.43$, $P = 0.05$, $\eta^2 = 0.20$] were not significantly different across conditions, whereas averaged summed errors [$F_{(1.45, 20.29)} = 47.87$, $P < 0.0001$, $\eta^2 = 0.77$], maximum velocity [$F_{(1.94, 27.10)} = 15.41$, $P < 0.0001$, $\eta^2 = 0.52$], and maximum force [$F_{(1.41, 19.76)} = 345$, $P < 0.0001$, $\eta^2 = 0.96$] were significantly different across conditions. Post hoc *t*-tests showed that maximum force, summed errors, and maximum velocities were significantly higher during motor adaptation compared to late familiarization (Supplementary Table 1, Supplementary Fig. 5).

Each participant made fewer errors in the final stages of motor adaptation, which was evident in fewer deviations from the ideal straight line (T1: 10.96 ± 4.70 cm > T2: 4.42 ± 1.28 cm), reflected by positive MLI values. At a group level, paired *t*-tests revealed that in T2 summed errors were significantly lower compared to T1 [$t_{(14)} = 5.60$, $P < 0.0001$, $\eta^2 = 3.40$]. The MLI (53 ± 22%)

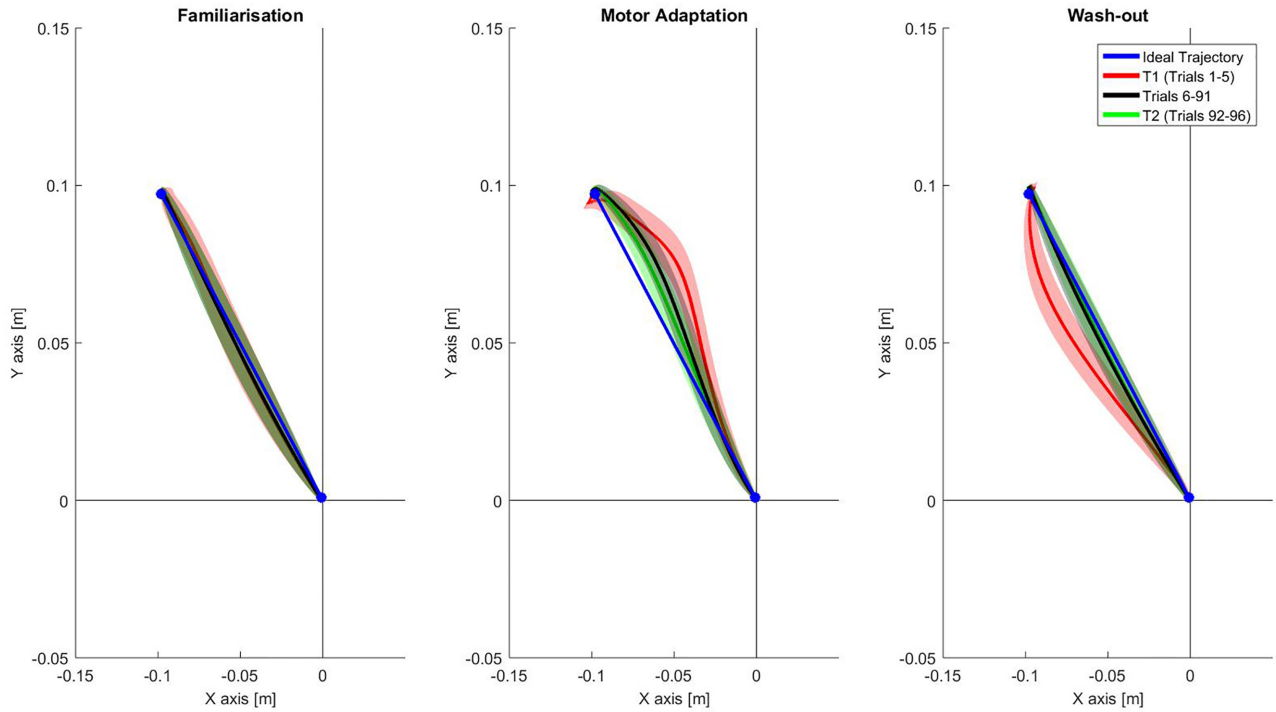

Figure 2: Movement trajectories during late familiarization, early motor adaptation, late motor adaptation, and late wash out. Group-level trajectories (shaded curve traces represent ± 1 SEM). In each condition. The blue line illustrates the ideal trajectory from the central starting point ($x = 0$; $y = 0$) to the peripheral target, the red line the average of the first five trials, the green line the average of the last five trials, and the grey line the average of the trials in between.

varied largely across participants ranging from 7.9 to 80.55% reflecting a high variability in motor learning capacity (Supplementary Fig. 6c).

EEG: N300 (ERN)

A negative deflection (N300) in fronto-central electrodes were observed around movement onset (330 ms) in all conditions (Fig. 3a). These deflections were larger during motor adaptation compared to non-adaptation conditions (late familiarization and late wash out). The N300 was largest in the fronto-central electrode FCz (Fig. 3b and Supplementary Fig. 7).

Repeated-measures ANOVA revealed a significant effect of condition in the N300 in electrodes mainly overlying central brain regions (Fig. 3A, B). Post hoc *t*-tests showed that N/P300 amplitudes were significantly larger during motor adaptation compared to familiarization.

Specifically, the N300 was larger during early motor adaptation compared to late familiarization in the following electrodes: bilateral fronto-central regions (Fp1, F3, Fz, F4, FC5, FC1, FC2, C3, Cz, CP6, AF7, AF3, AF4, F5, F1, F2, FC3, FCz, FC4, C1, C2, C6).

N300 was larger during late motor adaptation compared to late familiarization in the following electrodes: contralateral sensorimotor regions to the reaching arm (Fz, FC1, C3, Cz, CP1, CP6, FC3, FCz, C1, C6).

No significant difference in the N300 between early and late motor adaptation was detected.

There was a significant negative correlation between the MLI and N300 in early motor adaptation ($r = -0.62$, $P = 0.014$) and late motor adaptation ($r = -0.61$, $P = 0.015$). There was also a significant negative correlation between the MLI and the averaged N300 amplitude from early and late motor adaptation (in electrodes showing a significant modulation from late familiarization) ($r = -0.67$, $P = 0.006$), indicating that a larger N300 amplitude during motor adaptation is associated with higher MLI values (Fig. 4).

TMS-EEG: TEP N100 modulation

Single-pulse TMS to left M1 reliably produced identifiable negative and positive deflections in the EEG data. The N100 peak amplitude occurred in a time window between 75 and 150 ms post-TMS (Farzan *et al.*, 2013; Komssi *et al.*, 2002; Paus *et al.*, 2001). The N100 peak amplitude was significantly attenuated post-motor adaptation compared to premotor adaptation. The distribution and *t*-test scalp map for each electrode are plotted in scalp maps (Fig. 5A). The electrodes showing a significant modulation were mainly overlying sensorimotor regions: Fz, FC1, FC2, CZ, CP1, CP2, F2, FC3, FCz, F4, C1, C2, and P1. The averaged N100 amplitude of these electrodes was then calculated (Fig. 5B, C) and used for subsequent cortico-behavioral relationships.

The linear regression between the resting-state premotor adaptation N100 peak amplitude and the MLI showed that the premotor adaptation N100 peak

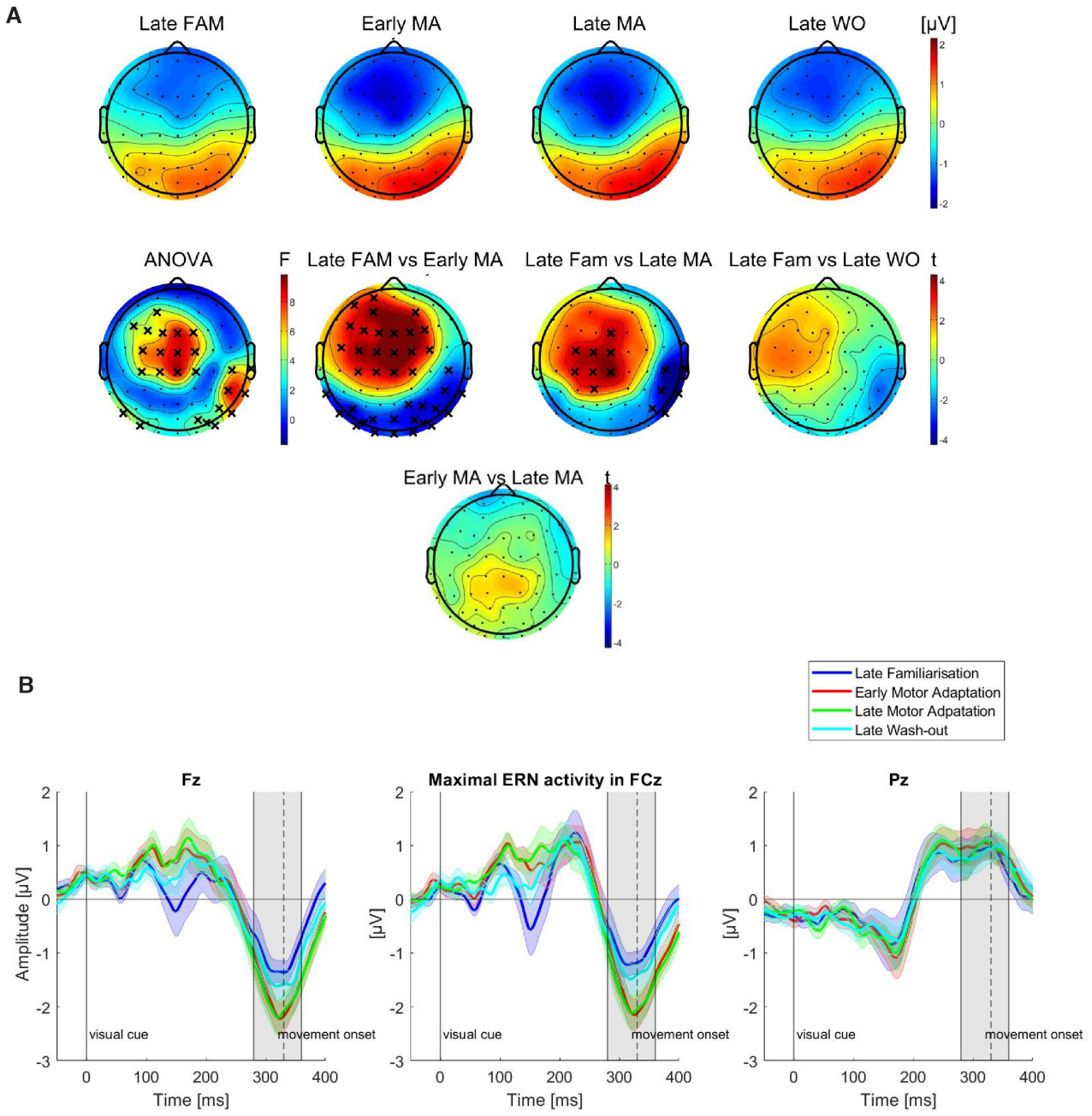

Figure 3: (**A**) N300 component. Scalp maps of N300 component: N300 amplitude (μV) in late familiarization, early motor adaptation, late motor adaptation, and late wash out. In the middle panel, scalp maps of the non-parametric permutation-based permutation repeated-measures ANOVA, followed by pairwise non-parametric permutation-based *t*-tests comparing late familiarization with all other conditions, as well as early and late motor adaptation are shown. Significance level was set to 0.05 for the ANOVA and to 0.0125 for the post hoc tests. All *P* values were FDR adjusted to control for multiple comparisons (63 electrodes) and significant electrodes are highlighted with a cross. In the *t*-statistics maps, blue shades represent a larger N300 amplitude compared to late familiarization, whereas red shades indicate decreased N300 amplitudes compared to late familiarization. (**B**) ERP average ($N = 15$, shaded curve traces represent ± 1 SEM) waveform in three representative electrodes showing the maximal activity around movement onset (330 ms post-visual cue). The N300 was extracted as mean amplitude between 280 and 360 ms post-visual cue (shaded grey area).

amplitude explained 35% of the variance [$R^2 = 0.35$, $F_{(1, 14)} = 7.09$, $P = 0.02$] and significantly predicted MLI of participants ($\beta = 32$, $P = 0.004$) (Fig. 6). Residuals were normally distributed (Supplementary Fig. 8).

Discussion

Motor adaptation to the forcefield environment and after effects on removal of the forcefield were observed. The magnitude of ERN activity was associated with the degree of motor adaptation, reflecting the formation of a

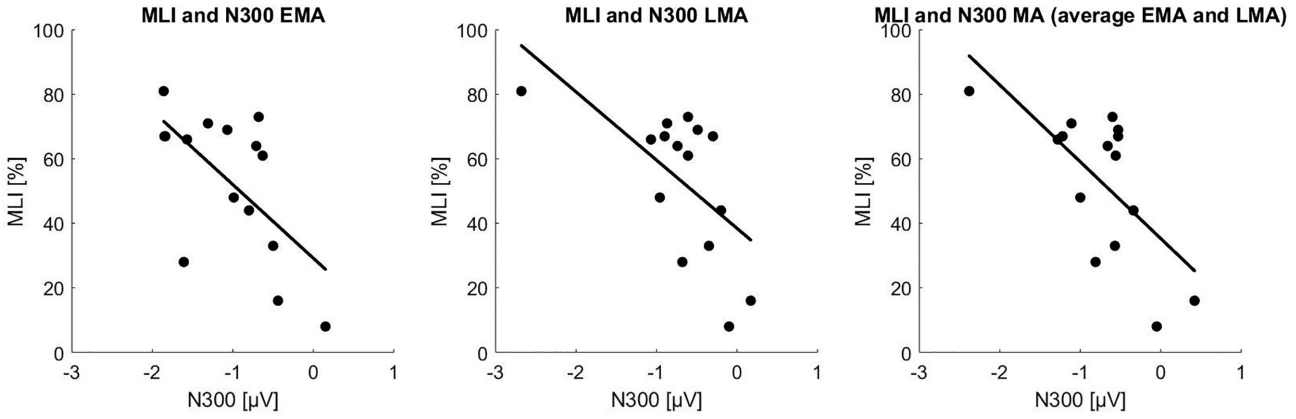

Figure 4: The association between the MLI and the N300 amplitude in early and late motor adaptation in the averaged electrodes showing a significant modulation from late familiarization. MLI was significantly negatively correlated with the N300 amplitude in early motor adaptation (average of significantly modulated electrodes compared to late familiarization) ($r = -0.62$, $P = 0.014$) and the late motor adaptation N300 amplitude (average of significantly modulated electrodes compared to late familiarization) ($r = -0.61$, $P = 0.015$). MLI was also significantly correlated with the averaged N300 amplitude from early and late motor adaptation (in electrodes showing a significant modulation from late familiarization) ($r = -0.67$, $P = 0.006$). (Bonferroni adjusted $P < 0.0167$, for three correlations).

predictive internal model adapted to the forcefield environment. Attenuation in TEP N100 amplitude post-motor adaptation relative to baseline was found, indicative of neuroplastic changes within sensorimotor regions, and baseline TEP N100 amplitude at rest predicted subsequent motor learning.

Participants learned to compensate for the mechanical perturbation, which was evident in the trial-by-trial decrease in trajectory errors during motor adaptation. Overshoot errors (after effects) were observed when the forcefield was unexpectedly removed, which represents the development of a predictive movement to overcome the previously expected applied forcefield (Hunter *et al.*, 2009). The compensation for the mechanical perturbation during motor adaptation and the after effects are two mechanisms that reflect the formation of an internal model of the dynamics of the motor adaptation task, which enables the prediction and compensation for the mechanical perturbation (Kawato and Wolpert, 1998; Shadmehr *et al.*, 2010; Thoroughman and Shadmehr, 2000). The internal models consist of a map of the dynamics of the motor task, which facilitates prediction and compensation in mechanical behaviour, and predictions in these internal models transform motor commands into sensory consequences, termed feed-forward mechanisms, to improve the ability to estimate the state of the body and the world around it (Shadmehr and Mussa-Ivaldi, 1994).

The N300 ERP component occurring around movement onset was increased during motor adaptation as compared to non-adapting conditions in fronto-central regions (Contreras-Vidal and Kerick, 2004). This component resembles the timing and scalp topography of the ERN, elicited after the onset of erroneous responses with maximal activity in fronto-central brain regions (Anguera *et al.*, 2009; Gehring *et al.*, 2018, 1993). The ERN is thought to originate in the ACC and pre-SMA and has been linked to error processing such as error monitoring, error correction, and performance improvement (Krigolson *et al.*, 2015; MacLean *et al.*, 2015). The ERN is increasingly activated during erroneous compared to correct responses (Holroyd and Coles, 2002; Krigolson *et al.*, 2015; MacLean *et al.*, 2015), however, the ERN has not only been observed during erroneous responses but also during correct responses around movement onset (Contreras-Vidal and Kerick, 2004; Krigolson and Holroyd, 2006).

In the present study, a negative deflection around movement onset in fronto-central regions was present in both adaptation and non-adaptation conditions. The negativity was larger during motor adaptation, however, when trajectory errors were significantly higher compared to non-adapting conditions (late familiarization and wash-out). Even though trajectory errors decreased during later stages of motor adaptation, they never reached baseline levels and were still significantly higher compared to late familiarization. Therefore, enhanced ERN activity during late motor adaptation compared to late familiarization was expected.

As ERN activity started before movement onset and peaked around movement onset (280–360 ms post-visual cue), it is unlikely to represent visual and proprioceptive feedback, which occurs around 50–150 ms post-movement onset (i.e. roughly 380–530 ms post-visual cue in the present study), but rather represents activity of the view of the limb before movement (MacLean *et al.*, 2015). At the start of the motor adaptation condition, a new forcefield is introduced and participants cannot predict the forcefield yet, but, with an increasing number of trials (i.e. in the later part of the early adaptation and the late adaptation condition), participants are already familiar with the forcefield and can learn to predict it, and adapt their movement to the forcefield (as can be seen by the reduction in errors). Given that neural activity N300 is seen before the movement starts before movement onset, we suggest that it reflects the formation prediction to the new environment (i.e. forcefield).

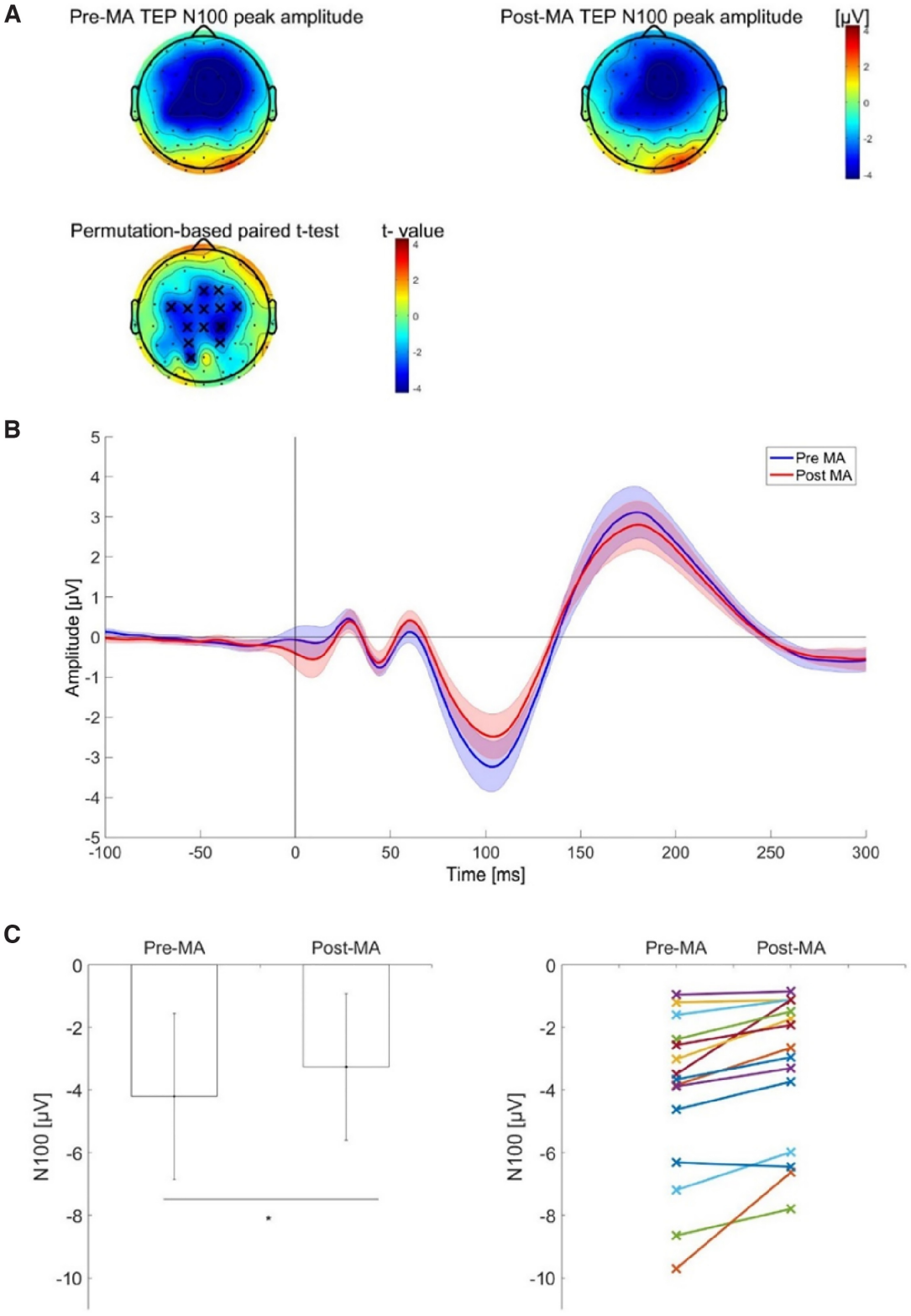

Figure 5: (**A**) TMS-evoked potentials (TEP) N100 time locked to TMS pulse pre- and post-motor adaptation. Top panel: scalp map of the TEP N100 peak amplitude extracted between 75 and 150 ms post-TMS in the upper panel (group averages $N = 15$). Lower panel: statistical *t*-maps of the permutation-based paired *t*-test between pre- and post-motor adaptation. Significant electrodes are highlighted with a cross. (**B**) Grand-average N100 TEP amplitude ($N = 15$, shaded area represents ± 1 SEM) in the averaged electrodes highlighted with a cross in the scalp map pre- and post-motor adaptation. The *x* axis represents time in ms from 100 pre-TMS to 300 ms post-TMS and the *y* axis the amplitude in μV. The solid vertical line represents the timing of the TMS pulse. (**C**) Bar plot (group-level N100, mean ± SD left panel) and line plot (single-participant N100; right panel) of the N100 peak amplitude in the averaged electrodes highlighted in the scalp map.

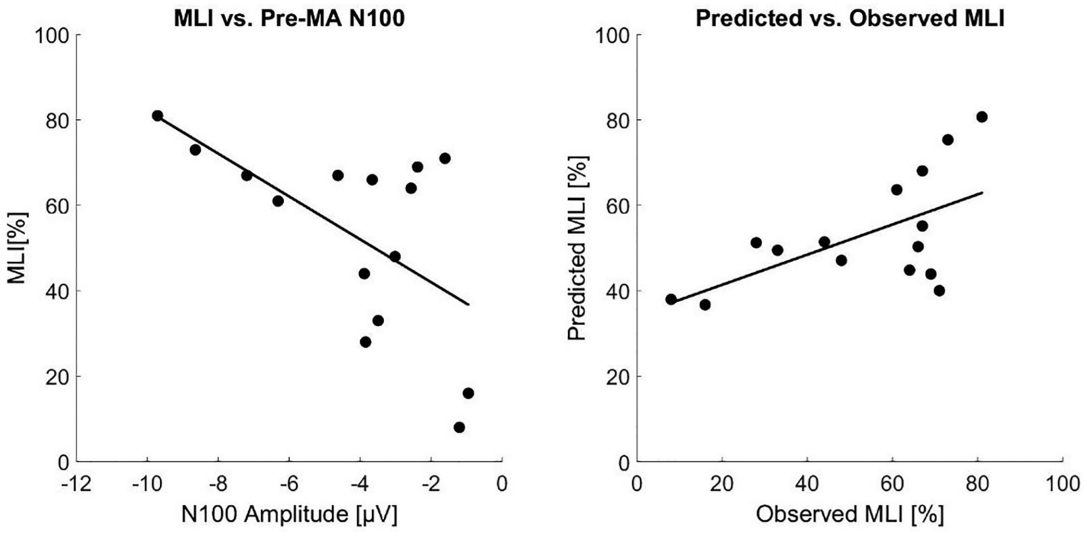

Figure 6: TEP N100 amplitude premotor adaptation and the MLI. Scatterplot between the N100 TEP amplitude premotor adaptation in the averaged electrodes and the MLI. The left panel depicts the MLI association against the N100 amplitude premotor adaptation in the averaged electrodes and the right panel the predicted MLI against the observed MLI. The simple linear regression revealed that the TEP N100 peak amplitude premotor adaptation was a significant predictor and explained 35% of the variance [$R^2 = 0.35$, $F_{(1, 14)} = 7.09$, $P = 0.02$] of the MLI ($\beta = 32$, $P = 0.004$).

Therefore, the ERN is likely to represent the formation of a predictive internal model of the novel environment adapted to the forcefield perturbation. This is consistent with the finding that the ERN during early and late motor adaptation correlated with performance improvements (smaller trajectory errors) during motor adaptation.

It can be proposed that the ERN observed in this study reflects performance monitoring to detect trajectory errors required to adapt the internal visuomotor representation to the perturbed environment. ERN is elicited by prediction errors, namely the comparison between the intended response with the predicted response, which are estimated from the output of an internal model activated by an efference copy of the motor command (Contreras-Vidal and Kerick, 2004; Holroyd and Coles, 2002). The findings indicate that the ERN reflected the successful formation of an internal predictive model adapted to the perturbed environment. Greater ERN activity was linked to better performance improvements (decreases in trajectory errors). Interestingly, the ERN seemed to be insensitive to error magnitude, since it did not correlate with the averaged trajectory errors during motor adaptation. The findings suggest that the ERN activity reflected a mechanism of error processing in which error information is used to improve performance rather than simply reflecting the error magnitude.

ERN amplitudes are attenuated and corresponded to lower error-correction rates in ACC lesions (Swick and Turken, 2002), suggesting a dissociation between error monitoring and detection. Crucially, even in the absence of an ERN production due to lesions in the medial prefrontal cortex, patients can still be aware of (i.e. detect) errors (Stemmer *et al.*, 2004). We propose that the ERN is linked to optimization strategies aiming to reduce errors rather than reflecting error detection and commission as there was a significant correlation between the ERN and performance improvement (higher MLI), but a lack of correlation between the ERN and net error magnitude.

Moran *et al.*'s (2017) meta-analysis reported that the ERN is larger in depression compared to healthy controls, while there were significant effects of task and population. The ERN has been proposed to be a common biomarker for internalizing disorders, including obsessive-compulsive and anxiety disorders (Riesel *et al.*, 2019). Increased anterior cingulate activity is a consistent predictor of clinical outcome in depression (Fu *et al.*, 2013). Psychomotor abnormalities are common in depression, and whether internal models associated with motor adaptation could be extrapolated to internal models associated with depressive symptomatology require investigation (Fu *et al.*, 2019), in which ACC function during error monitoring and cognitive control could reflect a common endophenotype in internalizing disorders (Reisel *et al.*, 2019). However, to develop clinically relevant biomarkers will require high accuracy at the level of the individual (Nouretdinov *et al.*, 2011).

Motor adaptation accompanied by sensorimotor plasticity

Motor adaptation leads to functionally specific changes in both motor and sensory regions, including in the primary motor cortex (M1), primary sensory motor cortex (S1), supplementary motor area, dorsal premotor cortex, and cerebellum (Vahdat *et al.*, 2011). Adaptation is thought to support motor recovery by reinforcing neural plasticity (Bastian, 2008, Basteris *et al.*, 2014).

As expected, forcefield adaptation was accompanied by changes in cortical excitability, which was indexed by

a significant modulation of the TEP N100 amplitude, a biomarker of inhibitory processes (Du *et al.*, 2018, Premoli *et al.*, 2014). The TEP N100 amplitude was significantly reduced post- compared to premotor adaptation over sensorimotor regions and was not restricted to M1. This finding corroborates previous TMS studies measuring corticomotor neuronal changes of excitability with MEPs (Ljubisavljevic, 2006) and expanding them to regions outside M1 by measuring changes in excitability on a whole scalp level with TEPs. The present study had applied TMS over M1 pre- and post-motor adaptation at rest and recorded TMS-evoked cortical responses from the whole scalp. Permutation-based whole scalp paired comparisons of the TEP N100 amplitude showed that significant modulations were seen over bilateral sensorimotor regions.

As N100 amplitude is believed to represent $GABA_B$-receptor activity (Premoli *et al.*, 2014); the underlying neuronal mechanisms of sensorimotor excitability changes, as measured with the N100 amplitude, probably reflect modulations of $GABA_B$-mediated inhibitory pathways. The present study suggests that decreases in the TEP N100 reflect GABA-related cortical inhibition decreases, which could be related to motor adaptation (Ljubisavljevic, 2006).

However, the behavioural and functional relevance of the observed sensorimotor plasticity remains to be elucidated, since the present study did not find a significant correlation between the change in cortical plasticity as measured by the percentage decrease of the N100 amplitude from pre- to post-motor adaptation and performance improvement during motor adaptation. The lack of association between sensorimotor plasticity and behavioural performance improvement could imply that the observed neuroplastic changes in sensorimotor cortical regions reflect an incomplete picture and that these changes could also, at least in part, be secondary to subcortical modulations, such as plasticity in the cerebellum that has a central role in motor adaptation (Krebs *et al.*, 1998; Spampinato and Block, 2017).

Moreover, driving neuroplasticity in the cerebellum by applying tDCS is associated with decreases in errors during adaptation, whereas tDCS over M1 has no behaviourally relevant effect (Galea *et al.*, 2011). The idea that motor adaptation not only engages distinct cortical regions but also a network of brain regions has been demonstrated by functionally specific changes in distinct resting state networks following motor adaptation (for a review, see Ostry and Gribble, 2016). For instance, Vahdat *et al.* (2011) distinguished specific networks related to perceptual changes comprising the second somatosensory cortex, ventral premotor cortex, and supplementary motor cortex from those relevant for motor aspects of learning including cerebellar cortex, the M1, and the dorsal premotor cortex. However, as EEG is unable to measure subcortical regions, such as the cerebellum, it might explain why the present study did not observe a direct relationship between plasticity changes and behavioural performance.

Native cortical excitability linked to motor learning performance

The present study examined how variations in intrinsic excitability measured with TMS-EEG at rest are related to performance improvement in motor adaptation. Larger N100 amplitudes predicted greater improvements in performance, suggesting that inhibitory mechanisms have a central role in motor adaptation. N100 amplitude was correlated and predictive of subsequent motor adaptation but not with the magnitude of errors at the start of motor adaptation, indicating the specificity of the relationship to motor learning and not to a baseline measurement of errors. Larger N100 amplitude measured at rest was associated with greater subsequent motor adaptation suggesting that greater cortical inhibitory activity is related with improved motor learning.

This might seem counter-intuitive, but as the N100 amplitude reflects GABAergic function, increased GABA levels at rest have been linked with poorer motor learning (Kolasinski *et al.*, 2019; Stagg *et al.*, 2011). It has also been reported that greater inhibition at the start of the motor task is associated with improved motor learning (Nowak *et al.*, 2017) and that higher GABA concentrations in M1 are related to improved motor performance reflected by faster reaction times (Greenhouse *et al.*, 2017). Furthermore, a lack of inhibition can lead to poorer motor performance and to disorders such as dystonia (Beck *et al.*, 2009; Stinear and Byblow, 2004).The association between higher inhibition before motor adaptation and better subsequent motor performance presented in this study suggests that a higher inhibitory capacity could be beneficial for motor learning, possibly due to increased precision of GABAergic transmission.

Motor learning and metaplasticity

Motor learning relies on the strengthening of horizontal connections within M1 (Rioult-Pedotti *et al.*, 1998, 2000) and most probably depend on LTP-like mechanisms (Ziemann, 2004). Metaplasticity refers to how neuronal changes can prime subsequent synaptic plasticity, the plasticity of neuroplasticity, which includes intrinsic features in neuronal membranes (Abraham and Bear, 1996). Potential strategies to boost motor learning include increasing the excitability of M1 during motor practice by weakening intracortical inhibitory circuits, referred to as 'gating', as well as lowering the threshold to induce synaptic plasticity by lowering neuronal activity (i.e. excitability) prior to motor learning, termed 'homeostatic metaplasticity' (Ziemann and Siebner, 2008). Hassanzahraee *et al.* (2018) report that the synaptic activity induced by priming protocols can modify the effects of the test protocol on corticospinal excitability. Neuroplasticity refers to the ability of the brain to continuously change structurally and functionally throughout an individual's life, which could be observed in changes such as neuronal responsiveness and synaptic connectivity, as

well as grey matter volume, and white matter structure (Hummel and Cohen, 2005, Voss *et al*., 2017).

The present finding of higher resting-state inhibitory (i.e. lower excitatory activity) as a predictor of better motor learning is consistent metaplasticity. If previous neuronal activity is low, homeostatic metaplasticity will tend towards an LTP-like effect, while if neuronal activity is high, then homeostatic metaplasticity will tend towards a LTD-like effect (Ziemann and Siebner, 2008). GABAergic inhibition affects plasticity thresholds and N100 is a marker of GABA function (Wigstrom, 1983). Individual differences in resting-state inhibitory capacity prior to motor adaptation contribute to the variability in motor performance improvement, and the TEP N100 amplitude could serve as a biomarker to harness these differences to best determine the potential of motor learning. Depending on the resting-state TEP N100 amplitude, an inhibitory or excitatory NIBS could be applied before motor learning to promote LTP-like mechanisms during motor adaptation and thus boost motor performance.

Hassanzahraee *et al*. (2018) review of the impact of paired associative brain stimulation of M1 on subsequent motor learning, demonstrates how an inhibitory paired associative brain stimulation (i.e. promoting LTD-like effects) applied before motor practice can enhance subsequent motor learning. Such an application in a clinical population could be incorporated to improve upper limb recovery. The predictive potential of the TEP N100 in motor learning capacity could potentially be used to understand the large inter-participant variability in motor learning and upper limb recovery in patients who have suffered a stroke (Davidson *et al*., 2016), as well as the significant clinical heterogeneity in major depression in which psychomotor abnormalities are prominent feature (Fu *et al*., 2019).

Limitations

TMS-evoked responses are contaminated by auditory evoked potentials produced by the loud clicking sound of the TMS pulse and somatosensory evoked potentials produced by the activation of the peripheral muscle contraction (Conde *et al*., 2019). Although white noise was used to mask the auditory artefact in the EEG data, it cannot be ruled out that the data were not contaminated with the artefact overlying the N100 amplitude. However, such an artefact would have affected all the experimental conditions in the same manner, so that any potential differences in N100 amplitude would reflect true neural differences and were not caused by this artefact. Furthermore, it is not possible to establish the specificity of N100 modulation to motor adaptation in the present design. Control conditions involving no perturbation or acquiring a measure of TMS evoked N100 following a wash-out period could assess the specificity of the effect to motor adaptation. Nonetheless, baseline N100, measured prior to motor adaptation, predicted the amount of error reduction during motor adaptation (i.e. motor learning index) as a measure of motor learning.

Conclusions

Individuals successfully formed an internal predictive model to the forcefield environment, allowing them to make accurate movements in a perturbed environment. Motor adaptation refers to the learning of a previously known motor skill in the presence of an additional perturbation. The formation of the internal model was reflected by ERN activity in fronto-central regions. Motor adaptation induced significant changes in cortical excitability over sensorimotor regions, suggesting that neuroplastic changes outside the M1 are also involved in motor adaptation mechanisms. The finding of a predictive value of the inhibitory biomarker TEP N100 on motor learning provides a theoretical interpretation that resting state motor cortical excitability contributes to individual variations in motor learning.

Supplementary Data

Supplementary data are available at *Psychoradiology* online.

Authors Contributions

Myriam Taga: Validation, formal analysis, investigation, data curation, and writing the original draft

Annacarmen Curci: Formal analysis

Sara Pizzamigglio: Writing; review and editing

Irene Lacal: Data curation

Duncan L. Turner: Conceptualization, resources, supervision, and funding acquisition

Cynthia H.Y. Fu: Supervision, writing the original draft, review and editing, and funding acquisition

Funding

This work was supported by a University of East London Excellence PhD scholarship to MT and in part from a Medical Research Council grant to CF (grant number G0802594).

Conflict of interest

None declared.

References

Abraham WC, Bear MF (1996) Metaplasticity: the plasticity of synaptic plasticity. *Trends Neurosci* **19**:126–30.

Anguera JA, Seidler RD, Gehring WJ (2009) Changes in performance monitoring during sensorimotor adaptation. *J Neurophysiol* **102**:1868–79.

Basteris A, Nijenhuis SM, Stienen AHA, *et al*. (2014) Training modalities in robot-mediated upper limb rehabilitation in stroke: a framework for classification based on a systematic review. *J NeuroEng Rehab* **11**:111.

Bastian AJ (2008) Understanding sensorimotor adaptation and learning for rehabilitation. *Curr Opin Neurol* **21**:628–33.

Beaulieu C, Bourassa MÈ, Brisson B, *et al.* (2014) Electrophysiological correlates of motor sequence learning. *BMC Neuroscience* **15**:102.

Beck S, Shamim EA, Pirio Richardson S, *et al.* (2009) Interhemispheric inhibition is impaired in mirror dystonia. *Eur J Neurosci* **29**:1634–40.

Benjamini Y, Yekutieli D (2001) The control of the false discovery rate in multiple testing under dependency. *Annals Stats* **29**:1165–88, August 2001.

Bonnard M, Spieser L, Meziane HB, *et al.*. (2009) Prior intention can locally tune inhibitory processes in the primary motor cortex: direct evidence from combined TMS-EEG. *Eur J Neurosci* **30**:913–23.

Conde V,Tomasevic L,Akopian I, *et al.* (2019) The nontranscranial TMS-evoked potential is an inherent source.

Contreras-Vidal JL, Kerick SE (2004) Independent component analysis of dynamic brain responses during visuomotor adaptation. *Neuroimage* **21**:936–45.

Davidson TW, Bolic M, Tremblay F (2016) Predicting modulation in corticomotor excitability and in transcallosal inhibition in response to anodal transcranial direct current stimulation. *Front Hum Neurosci* **10**:49.

Delorme A, Makeig S (2004) EEGLAB: an open source toolbox for analysis of single-trial EEG dynamics including independent component analysis. *J Neurosci Methods* **134**:9–21.

Desmurget M, Grafton S (2000) Forward modeling allows feedback control for fast reaching movements. *Trends Cogn Sci* **4**:423–31.

Diedrichsen J, Hashambhoy Y, Rane T, *et al.* (2005) Neural correlates of reach errors. *J Neurosci* **25**:9919–31.

Du X, Rowland LM, Summerfelt A, *et al.* (2018) TMS evoked N100 reflects local GABA and glutamate balance. *Brain Stimulation*:1071–9.

Faiman I, Pizzamiglio S, Turner DL (2018) Resting-state functional connectivity predicts the ability to adapt arm reaching in a robot-mediated forcefield. *Neuroimage* **174**: 494–503.

Falkenstein M, Koshlykova NA, Kiroj VN, *et al.* (1995) Late ERP components in visual and auditory go/no go tasks. *Electroencephalogr Clin Neurophysiol/Evoked Pot* **96**:36–43.

Farzan F, Barr MS, Hoppenbrouwers SS, *et al.* (2013) The EEG correlates of the TMS-induced EMG silent period in humans. *Neuroimage* **83**:120–34.

Farzan F, Vernet M, Shafi MMD, *et al.* (2016) Characterizing and modulating brain circuitry through transcranial magnetic stimulation combined with electroencephalography. *Front Neural Circuits* **10**:73.

Fields E, Kuperberg GR (2018) Having your cake and eating it too: flexibility and power with mass univariate statistics for ERP data.

Frank MJ, Woroch BS, Curran T (2005) Error-related negativity predicts reinforcement learning and conflict biases. *Neuron* **47**:495–501.

Fu CHY, Fan Y, Davatzikos C (2019) Addressing heterogeneity (and homogeneity) in treatment mechanisms in depression and the potential to develop diagnostic and predictive biomarkers. *NeuroImage: Clinical* **24**:101997.

Fu CHY, Steiner H, Costafreda SG (2013) Predictive neural biomarkers of clinical response in depression: a meta-analysis of functional and structural neuroimaging studies of pharmacological and psychological therapies. *Neurobiol Dis* **52**:75–83.

Galea JM, Vazquez A, Pasricha N, *et al.* (2011) Dissociating the roles of the cerebellum and motor cortex during adaptive learning: the motor cortex retains what the cerebellum learns. *Cereb Cortex* **21**:1761–70.

Gehring WJ, Goss B, Coles MGH, *et al.* (2018) The error-related negativity. *Perspect Psychol Sci* **13**:200–4.

Gehring WJ, Goss B, Coles MGH, *et al.* (1993) A neural system for error detection and compensation. *Psychol Sci* **4**:385–90.

Greenhouse I, King M, Noah S, *et al.* (2017) Individual differences in resting corticospinal excitability are correlated with reaction time and GABA content in motor cortex. *J Neurosci* **37**:2686–96.

Haith AM, Krakauer JW (2013) Model-based and model-free mechanisms of human motor learning. *Adv Exp Med Biol* **782**:1–21.

Hassanzahraee M, Zoghi M, Jaberzadeh S (2018) How different priming stimulations affect the corticospinal excitability induced by noninvasive brain stimulation techniques: a systematic review and meta-analysis. *Rev Neurosci* **29**: 883–99.

Holroyd CB, Coles MGH (2002) The neural basis of human error processing: reinforcement learning, dopamine, and the error-related negativity. *Psychol Rev* **109**:679–709.

Hummel FC, Cohen LG (2005) Drivers of brain plasticity. *Curr Opin Neurol* **18**:667–74.

Hunter T, Sacco P, Nitsche MA, *et al.* (2009) Modulation of internal model formation during forcefield-induced motor learning by anodal transcranial direct current stimulation of primary motor cortex. *J Physiol* **587**:2949–61.

Jasper H (1958) Progress and problems in brain research. *J Mt Sinai Hosp N Y* **25**:244–53.

Kawato M, Wolpert D (1998) Internal models for motor control. *Novartis Found. Symp* **218**:291–307.

Kolasinski J, Hinson EL, Divanbeighi Zand AP, *et al.* (2019) The dynamics of cortical GABA in human motor learning. *J Physiol* **597**:271–82.

Komssi S, Kähkönen S, Ilmoniemi RJ (2004) The effect of stimulus intensity on brain responses evoked by transcranial magnetic stimulation. *Hum Brain Mapp* **21**:154–64.

Komssi S, Aronen HJ, Huttunen J, *et al.* (2002) Ipsi-and contralateral EEG reactions to transcranial magnetic stimulation. *Clin Neurophysiol* **113**:175–84.

Korhonen RJ, Hernandez-Pavon JC, Metsomaa J, *et al.* (2011) Removal of large muscle artifacts from transcranial magnetic stimulation-evoked EEG by independent component analysis. *Med Biol Eng Comput* **49**:397–407.

Krakauer JW, Mazzoni P (2011) Human sensorimotor learning: adaptation, skill, and beyond. *Curr Opin Neurobiol* **21**:636–44.

Krebs HI, Brashers-Krug T, Rauch SL, *et al.* (1998) Robot-aided functional imaging: application to a motor learning study. *Hum Brain Mapp* **6**:59–72.

Krigolson OE, Cheng D, Binsted G (2015) The role of visual processing in motor learning and control: insights from electroencephalography. *Line Vis. Control Action* **110**:277–85.

Krigolson OE, Holroyd CB (2006) Evidence for hierarchical error processing in the human brain. *Neuroscience* **137**:13–7.

Ljubisavljevic M (2006) Transcranial magnetic stimulation and the motor learning-associated cortical plasticity. *Exp Brain Res* **173**:215–22.

MacLean SJ, Hassall CD, Ishigami Y, *et al.* (2015) Using brain potentials to understand prism adaptation: the error-related negativity and the P300. *Frontiers in Human Neuroscience* **9**:335.

Moran TP, Schroder HS, Kneip C, *et al.* (2017) Meta-analysis and psychophysiology: a tutorial using depression and

action-monitoring event-related potentials. *Int J Psychophysiol* **111**:17–32.

Mutanen TP, Biabani M, Sarvas J, *et al.* (2020)Source-based artifact-rejection techniques available in TESA, an open-source TMS–EEG toolbox *Brain Stimulation* **13**:1349–51.

Nouretdinov I, Costafreda SG, Gammerman A, *et al.* (2011) Machine learning classification with confidence: application of transductive conformal predictors to MRI-based diagnostic and prognostic markers in depression. *Neuroimage* **56**:809–13.

Nowak M, Hinson E, van Ede F, *et al.* (2017) Driving human motor cortical oscillations leads to behaviorally relevant changes in local GABAA inhibition: a tACS-TMS study. *J Neurosci* **37**:4481–92.

Oldfield RC (1971) The assessment and analysis of handedness: the Edinburgh inventory. *Neuropsychologia* **9**:97–113.

Ostry DJ, Gribble PL (2016) Sensory plasticity in human motor learning. *Trends Neurosci* **39**:114–23.

Ozdenizci O, Yalcin M, Erdogan A, *et al.* (2017) Electroencephalographic identifiers of motor adaptation learning. *J Neural Eng* **14**:046027.

Paus T, Sipila PK, Strafella AP (2001) Synchronization of neuronal activity in the human primary motor cortex by transcranial magnetic stimulation: an EEG study. *J Neurophysiol* **86**:1983–90.

Patton JL, Mussa-Ivaldi FA (2004) Robot-assisted adaptive training: custom forcefields for teaching movement patterns. *IEEE Trans Biomed Eng* **51**:636–46.

Patton JL, Stoykov ME, Kovic M, *et al.* (2006) Evaluation of robotic training forces that either enhance or reduce error in chronic hemiparetic stroke survivors. Exp. *Exp Brain Res* **168**:368–83.

Pizzamiglio S, Desowska A, Shojaii P, *et al.* (2017) Muscle co-contraction patterns in robot-mediated forcefield learning to guide specific muscle group training. *NeuroRehabilitation* **41**:17–29.

Premoli I, Castellanos N, Rivolta D, *et al.* (2014) TMS-EEG signatures of GABAergic neurotransmission in the human cortex. *J Neurosci* **34**:5603–12.

Riesel A, Klawohn J, Grützmann R *et al.* (2019) Error-related brain activity as a transdiagnostic endophenotype for obsessive-compulsive disorder, anxiety and substance use disorder. *Psychol Med* **49**:1207–17.

Ridding MC, Rothwell JC (2007) Is there a future for therapeutic use of transcranial magnetic stimulation? *Nat Rev Neurosci* **8**:559–67.

Rioult-Pedotti MS, Friedman D, Donoghue JP (2000) Learning-induced LTP in neocortex. *Science* **290**:533–6.

Rioult-Pedotti MS, Friedman D, Hess G, *et al.* (1998) Strengthening of horizontal cortical connections following skill learning. *Nat Neurosci* **1**:230–4.

Rogasch NC, Thomson RH, Farzan F, *et al.* (2014) Removing artefacts from TMS-EEG recordings using independent component analysis: importance for assessing prefrontal and motor cortex network properties. *Neuroimage* **101**:425–39.

Rogasch NC, Sullivan C, Thomson RH, *et al.* (2017) Analysing concurrent transcranial magnetic stimulation and electroencephalographic data: a review and introduction to the open-source TESA software. *Neuroimage* **147**:934–51.

Rossi S, Hallett M, Rossini PM, *et al.* (2009) Safety, ethical considerations, and application guidelines for the use of transcranial magnetic stimulation in clinical practice and research. *Clin Neurophysiol* **120**:2008–39.

Scott SH, Cluff T, Lowrey CR, *et al.* (2015) Feedback control during voluntary motor actions. *Curr Opin Neurobiol* **33**:85–94.

Shadmehr R, Mussa-Ivaldi FA (1994) Adaptive representation of dynamics during learning of a motor task. *J Neurosci* **14**:3208–24.

Shadmehr R, Smith MA, Krakauer JW (2010) Error correction, sensory prediction, and adaptation in motor control. *Annu Rev Neurosci* **33**:89–108.

Spampinato DA, Block HJ (2017) Cerebellar-M1 connectivity changes associated with motor learning are somatotopic specific. **37**:2377–86.

Spieser L, Meziane HB, Bonnard M (2010) Cortical mechanisms underlying stretch reflex adaptation to intention: a combined EEG–TMS study. *Neuroimage* **52**:316–25.

Stagg CJ, Bachtiar V, Johansen-Berg H (2011) The role of GABA in human motor learning. *Curr Biol* **21**:480–4.

Stemmer B, Segalowitz SJ, Witzke W, *et al.* (2004) Error detection in patients with lesions to the medial prefrontal cortex: an ERP study. *Neuropsychologia* **42**:118–30.

Stinear CM, Byblow WD (2004) Impaired modulation of intracortical inhibition in focal hand dystonia. *Cereb Cortex* **14**:555–61.

Swick D, Turken U (2002) Dissociation between conflict detection and error monitoring in the human anterior cingulate cortex. *Proc Natl Acad Sci USA* **99**:16354–9.

Thoroughman KA, Shadmehr R (2000) Learning of action through adaptive combination of motor primitives. *Nature* **407**:742–7.

Torrecillos F, Albouy P, Brochier T, *et al.* (2014) Does the processing of sensory and reward-prediction errors involve common neural resources? evidence from a frontocentral negative potential modulated by movement execution errors. *J Neurosci* **34**:4845–56.

Vahdat S, Darainy M, Milner TE, *et al.* (2011) Functionally specific changes in resting-state sensorimotor networks after motor learning. *J Neurosci* **31**:16907–15.

Voss P, Thomas ME, Cisneros-Franco JM, *et al.* (2017) Dynamic brains and the changing rules of neuroplasticity: implications for learning and recovery. *Frontiers in Psychology* **8**:1657–.

Wigström HGB (1983) Facilitated induction of hippocampal long-lasting potentiation during blockade of inhibition. *Nature* **301**:603–4.

Wolpert DM, Miall RC, Kawato M (1998) Internal models in the cerebellum. *Trends Cogn Sci* **2**:338–47.

Ziemann U (2017) Thirty years of transcranial magnetic stimulation: where do we stand? *Exp Brain Res* 1–12.

Ziemann ULF (2004) TMS induced plasticity in human cortex. *Rev Neurosci* **15**:253–66.

Ziemann U, Siebner HR (2008) Modifying motor learning through gating and homeostatic metaplasticity. *Brain Stimulation* **1**: 60–6.